

1 **Evaluating the geothermal heat pump potential from a thermostratigraphic assessment**
2 **of rock samples in the St. Lawrence Lowlands, Canada**

3

4 *Jasmin Raymond^{1,2}, Cédric Sirois¹, Maher Nasr¹ and Michel Malo¹*

5 *1- Institut national de la recherche scientifique, Centre Eau Terre Environnement, 490 de la*
6 *Couronne, Québec (Québec) Canada G1K 9A9*

7 *2- jasmin.raymond@inrs.ca; T: +1 418 654 2559; F: + 1 418 654 2600*

8

9 **Abstract**

10 The installation cost and the performance of geothermal heat pump systems are influenced by
11 the thermal state and properties of the subsurface. The ground ability to transfer heat
12 described by thermal conductivity is a dominant factor affecting the favorability of closed-
13 loop ground heat exchangers installed in vertical boreholes. A study that aimed at evaluating
14 the geothermal heat pump potential by mapping the thermal conductivity of rock sequences
15 was, therefore, performed for the St. Lawrence Lowlands sedimentary basin in Canada.
16 Thermal conductivity was measured in the laboratory on rock samples collected in outcrops
17 and used to complete design calculations of a geothermal system with a single borehole.
18 Results allowed the definition of thermostratigraphic units that can be linked to depositional
19 environments. Basal quartz-rich sandstones formed in a rift environment show a high
20 geothermal potential. Overlying dolomites, argillaceous limestones and shales deposited in a
21 passive margin evolving to a foreland basin exhibit a transition toward the top from high to
22 low geothermal potential. Upper turbidites and molasses have a moderate geothermal
23 potential. The thermal conductivity of the thermostratigraphic units is dominantly influenced
24 by the mineralogy of the sedimentary rocks. Understanding their origin is a key to improve
25 geothermal resource assessment and system design to anticipate new installations in the area.

26

27 **Key Words:** geothermal, heat pump, thermostratigraphy, thermal conductivity, sedimentary
28 basin, St. Lawrence Lowlands, Canada.

29

30

31 **1 Introduction**

32 Geothermal heat pump systems, also named ground source heat pumps, are one of the most
33 energy efficient alternatives for heating and cooling buildings (Self et al. 2013). This
34 technology relies on the Earth acting as a heat source or sink to maintain building
35 temperatures. The economic viability of vertical systems, where the heat pump is linked to
36 closed-loop ground heat exchangers (GHEs) installed in boreholes, can be affected by the
37 thermal state and properties of the subsurface. In this context, space heating and cooling are
38 influenced by the ground conditions that can be better understand to improve this human
39 activity. In fact, the length of ground heat exchanger required to fulfill the building energy
40 needs is commonly computed with a sizing equation taking into account the subsurface
41 temperature, heat capacity and thermal conductivity (Bernier 2000). Simulating the system
42 operating temperature to evaluate its performance and energy savings also relies on those
43 three parameters (Bernier 2001). The amount and the capacity of tools available to size and
44 simulate the operation of geothermal systems have increased over the past decade. The recent
45 development of analytical and numerical approaches to simulate ground coupled heat pump
46 systems documented in numerous studies outlines the growing interest in this field (Al-
47 Khoury et al. 2005; Al-Khoury and Bonnier 2006; Lamarche and Beauchamp 2007a;
48 Lamarche and Beauchamp 2007b; Cui et al. 2008; Lee and Lam 2008; Lamarche 2009; Li and
49 Zheng 2009; Philippe et al. 2009; Yang et al. 2010; Li et al. 2015; Wang et al. 2015).

50 Regardless of the approach used, it is critical to supply models with reliable subsurface
51 parameters. Temperature of the shallow subsurface can be found throughout the scientific
52 literature and databases, with data originating from boreholes (Majorowicz et al. 2009) or
53 inferred from the meteorological record (Signorelli and Kohl 2004). In the case of large
54 geothermal heat pump systems, where local variations in subsurface temperature may impact
55 the system design, the subsurface temperature can be measured in a pilot GHE (Gehlin and
56 Nordell 2003).

57 Estimation of the subsurface volumetric heat capacity is also straightforward as this parameter
58 is relatively uniform within different rock types for the temperature and pressure conditions
59 expected in the shallow subsurface (Clauser 2014a). The sensitivity of geothermal system
60 simulation models with respect to heat storage is additionally less important than that of
61 conductive heat transfer, allowing the toleration of an uncertainty in the evaluation of the
62 subsurface volumetric heat capacity. Appropriate estimation of this parameter can be obtained
63 knowing the dominant mineral phases of the rock formations or with a geological description

64 of the rock type to classify the subsurface heat storage potential (Waples and Waples 2004a,
65 b).

66 The evaluation of the subsurface thermal conductivity can be more challenging because this
67 parameter varies significantly among rock types, typically on a scale of 0.5 to $8 \text{ W m}^{-1} \text{ K}^{-1}$ at
68 the temperature and pressure conditions of the shallow subsurface (Clauser 2014b). The
69 porosity, water content and the mineral phases, which can be highly heterogeneous, are the
70 main factors affecting the subsurface thermal conductivity (Clauser and Huenges 1995;
71 Clauser 2006). Sedimentary rocks, which are of interest to this research, can have a low
72 thermal conductivity in the range of 0.5 to $2 \text{ W m}^{-1} \text{ K}^{-1}$ when having a marine origin, while
73 sedimentary rocks of terrestrial and chemical origins most commonly have a moderate
74 thermal conductivity between 2 to $4 \text{ W m}^{-1} \text{ K}^{-1}$ (Clauser 2014b). A high thermal conductivity
75 above $4 \text{ W m}^{-1} \text{ K}^{-1}$ is associated to quartz-rich specimens. Thermal response tests have been
76 proposed to assess the subsurface thermal conductivity in a pilot GHE before designing a
77 system (Rainieri et al. 2011; Raymond et al. 2011; Spitler and Gehlin 2015). The test has
78 grown in popularity for designing large ground-coupled heat pump systems, but can remain
79 uneconomical for smaller systems where the test cost is above the economic uncertainty
80 related to an unknown subsurface (Robert and Gosselin 2014). The need to map the
81 distribution of the subsurface thermal conductivity to help design smaller systems or for
82 screening simulations of larger systems is growing with increasing installations of GHEs. For
83 example, regional mapping of the subsurface thermal conductivity has been undertaken in
84 southern Italy, providing field data to guide geothermal designers (Di Sipio et al. 2014). A
85 methodology was then developed to estimate the geothermal potential in this region of Italy
86 based on geological information and simulation of geothermal heat pump systems (Galgaro et
87 al. 2015). Similar attempts to map the geothermal heat pump potential were conducted
88 (Casasso and Sethi 2016; De Filippis et al. 2015; Ondreka et al. 2007; Santilano et al. 2015;
89 Teza et al. 2015) but mostly rely on inferred subsurface thermal conductivity defined with
90 calculations constrained from geological information. In these studies, the geothermal
91 potential is commonly tied to the subsurface thermal conductivity, highlighting the need to
92 collect reliable field data to better assess this property among geological units. Populated
93 regions with expected system installations are priorities for further case studies.

94 An assessment of the subsurface thermal conductivity in the St. Lawrence Lowlands (SLL)
95 located in the province of Quebec, Canada, is presented in this study. The objective was to
96 evaluate the geothermal heat pump potential of the rock units of this sedimentary basin from

97 laboratory measurements of thermal conductivity. The geothermal potential was evaluated
98 with respect to ground-coupled heat pump systems where the heat exchangers are closed-
99 loops installed in boreholes, which are the most common geothermal systems in the SLL. This
100 potential was therefore linked to the length of borehole needed for a given system to be
101 installed in the area, which is mostly affected by the thermal conductivity of the host rock
102 when comparing similar building loads or energy demand. The information presented
103 provides the basis for a first assessment of the subsurface thermal conductivity at a regional
104 scale in the SLL. The collected data set, submitted as a supplementary material, is believed to
105 be an original contribution that can facilitate geothermal system design based on a
106 thermostratigraphic classification of rock units. The concept of thermostratigraphy is further
107 discussed in the context of geothermal heat pump systems.

108 **2 Geological settings**

109 The SLL forms a sedimentary basin covering ~20 000 km² to the south of Quebec province
110 (Figure 1). The region studied includes major cities such as Montreal and Quebec City and
111 has the highest population density in the province. The type of geothermal heat pump system
112 that is most commonly installed in the area is vertical closed-loops (Canadian GeoExchange
113 Coalition 2012).

114 The sedimentary basin of the SLL is located between the Precambrian basement of the
115 Grenville geological province and the Appalachians. The Precambrian basement is constituted
116 of metamorphosed igneous rocks dominated by gneisses with other igneous and metamorphic
117 rocks (Globensky 1987). Cambrian-Ordovician rocks of the Appalachian mountain belt are
118 mostly sedimentary in origin and have experienced a highly variable degree of metamorphism
119 and deformation.

120 The Cambrian-Ordovician rocks of the SLL basin formed in a geodynamic context evolving
121 from a rift to a passive margin and a foreland basin (Figure 2; Comeau et al. 2012). The rock
122 strata are relatively non-deformed and well preserved. A large synclinal elongated in the
123 Southwest-Northeast direction is the main structure associated to the SSL basin (Figure 3).
124 Steeply southeast dipping normal faults with a southwest-northeast direction affect the
125 sedimentary sequences, deepening and thickening towards the southeast (Castonguay et al.
126 2010). Logan's Line, a major thrust fault zone, delineates the southeastern boundary of the
127 SLL basin, which extends under the Appalachians (Figure 3).

128 Depositional environments influenced the formation of the sedimentary groups in the SLL
129 basin having distinct mineralogical phases and porosity values, from clay to quartz rich with
130 low to moderate porosity, where changes in rock type are expected to affect the geothermal
131 potential. The basal sandstone of the Potsdam Group unconformably overlies the crystalline
132 basement outcropping at surface toward the Northwest of the SLL basin. This group encloses
133 the Covey Hill Formation of fluvial origin, constituted of 80 to 98 % quartz and 3 to 10 %
134 plagioclase, as well as the homogenous Cairnside Formation deposited in a shallow subtidal
135 marine to marine deltaic environment and containing more than 98 % quartz (Globensky
136 1987). The average porosity of the Potsdam Group is between 4 to 6 % and values can locally
137 exceed 10 % (Tran Ngoc et al. 2014), which can affect its geothermal potential.

138 The Potsdam Group is overlain by the Beekmantown Group constituted of the Theresa
139 Formation, deposited in a marine environment, and the Beauharnois Formation, deposited in
140 lagoonal, intertidal and supratidal environments (Globensky 1987). At its base, the Theresa
141 Formation is made of quartz and dolomitic sandstone, with occasional dolostone increasing in
142 thickness toward the top of the formation and where sandstone thickness oppositely decreases.
143 The Theresa Formation is conformably overlain by the Beauharnois Formation made of
144 dolostone. The Beekmantown Group has an average porosity of 1~2 % (Tran Ngoc et al.
145 2014). The transition observed in the Beekmantown Group, from quartz-rich sandstone at the
146 base to dolostone at the top is seen to affect the geothermal potential changing from the
147 Theresa Formation to the Beauharnois Formation.

148 The Chazy, Black River and Trenton groups, unconformably overlying the Beauharnois
149 Formation represent shallow to deep marine environment deposits showing a deepening
150 upward trend (Lavoie 1994). These groups are dominantly constituted of limestone and
151 argillaceous limestone, with occasional dolostone and sandstone. The carbonate content is the
152 main factor affecting the geothermal potential.

153 Near the top of the Trenton Group, limestone decreases at the expense of the increasing clay
154 until the overlying Utica Shale (Globensky 1987). This transition marks a change toward a
155 deep marine depositional environment resulting in an increase of clay that can reduce the
156 geothermal potential in the Utica Shale. The Sainte-Rosalie Group, subsequently overlying
157 the Utica Shale, comprises siltstone, mudstone, silty mudstone and occasionally dolostone
158 showing a shallowing-upward trend with decreasing clay content toward the top (Globensky
159 1987).

160 The Lorraine Group, made of shale, sandstone, siltstone and limestone, overlies the Sainte-
161 Rosalie Group, both of which are turbidites. Molasses of the Queenston Group, on top of the
162 Lorraine Group, are characteristics of a continental to a subaerial deltaic environment
163 (Globensky 1987). Shale with minor sandstone and siltstone including occasional gypsum and
164 anhydrite lenses constitutes the Queenston Group. The heterogeneous rock types of both the
165 Lorraine and Queenstone groups may result in a varying geothermal potential.

166

167 Cretaceous intrusions called the Monteregians Hills crosscut the sedimentary sequence of the
168 SLL basin in the southwestern region (Figure 3). They are composed of a large variety of
169 igneous rocks, mostly pyroxenite, gabbro, diorite and pulaskite (Brisebois and Brun 1994).
170 The Monteregians Hills are surrounded by dike systems and have been brought to surface by
171 erosion during the Quaternary glaciations. Igneous rocks of the Monteregian Hills cover a
172 limited area near the surface and have not been considered in this regional assessment of the
173 subsurface thermal conductivity focusing on the sedimentary sequences as a first step.

174 Host rocks to the south of Quebec are commonly covered by unconsolidated Quaternary
175 deposits originating from the melt of the last ice cap giving birth to the Champlain Sea, which
176 covered older quaternary deposits of preceding glaciations (Globensky 1987). The
177 unconsolidated deposits are made of clay, sand and till and have a varying thickness ranging
178 from less than 5 m to more than 35 m. The thickness and the nature of the Quaternary
179 deposits can be found in water well records and groundwater databases available for the area,
180 for example the reports of Carrier et al. (2013) and Laroque et al. (2015). The unconsolidated
181 deposits have not been incorporated in this geothermal potential assessment since their
182 thickness varies significantly across the sedimentary basin. This work aimed at identifying
183 regional trends in thermal conductivity that can influence the operation of vertical ground-
184 coupled heat pump systems and was therefore focused on bedrock characteristics. The
185 information presented can be combined with site characteristics, such as overburden thickness
186 and nature, as geothermal heat pump systems are installed to complete system design based
187 on local geological settings. The groundwater level in the SLL basin is relatively shallow and
188 commonly found less than 10 m below the surface (Carrier et al. 2013; Laroque et al. 2015).
189 All host rocks were therefore assumed to be fully saturated.

190 This description of the SLL basin provides a qualitative understanding of the main factors
191 affecting the conductive heat transfer potential of the rock units, in which ground-coupled
192 heat pump systems can be installed and where further laboratory testing was carried out.

193 **3 Methodology**

194 The work to evaluate the geothermal heat pump potential of the SLL basin consisted in
195 collecting rock samples from outcrops, evaluating their thermal properties in the laboratory
196 and determining the length of borehole that would be needed for a small size ground-coupled
197 heat pump system with a single GHE. The measured thermal conductivities were compared
198 and originally grouped into thermostratigraphic units, defined in this study as consecutive
199 geological layers of similar conductive heat transfer ability. Sedimentary groups or formations
200 were combined or divided to define the thermostratigraphic units that are further constrained
201 by their positions within the sedimentary sequence. This definition is in agreement with
202 thermostratigraphic principles used for exploration of deep geothermal resources for power
203 generation (Gosnold et al. 2012; Sass and Götz 2012) and has been applied in this study to
204 ground-coupled heat pump systems. The borehole length obtained by sizing a typical system,
205 in which the thermal properties of the samples are input parameters, were compared and
206 assigned a low, medium and high geothermal potential to identify the favorability of the
207 thermostratigraphic units. Due to the territory covered and the difficulties to interpolate
208 thermal conductivity values, results were presented on point maps plotted on top of a
209 geological map of the SLL basin to visualize the extent and potential of the
210 thermostratigraphic units.

211 **3.1 Fieldwork**

212 A field campaign was conducted to visit outcrops and collect fifty rock samples representative
213 of each group constituting the sedimentary sequence of the SLL basin (Nasr et al. 2015).
214 Samples were collected from sedimentary beds that appeared most abundant when visiting
215 referenced outcrops that have been studied to define the stratigraphy of the area (Globensky
216 1987). Forty-five samples were suitable for analysis, which included at least three samples per
217 sedimentary group. A few samples from the proximal Grenville and Appalachian provinces
218 were also collected for comparison purposes. However, more samples would be required to
219 picture the diversity of rock types present in these complex geological provinces to fully
220 assess their geothermal potential. The size of the samples was generally more than 15~20 cm
221 in diameter, to allow measurement of thermal conductivity in the laboratory with a needle
222 probe.

223 **3.2 Laboratory measurements**

224 Collected samples were initially cut and a hole was drilled at the middle of the samples. The
225 size of the needle used for thermal conductivity measurements, and consequently the holes
226 drilled in the samples, was 3.8 mm in diameter and 60 mm in length. The samples were
227 allowed to cool down after drilling for at least a week before conducting thermal conductivity
228 measurements. The probe used was a KD2 pro model from Decagon Devices and encloses
229 one temperature sensor at the center of the needle having a heat injection rate equal to
230 6 W m^{-1} . Many of the samples broke while drilling the holes, especially friable clays. The
231 analyses were consequently performed on rock samples that were well consolidated and in
232 which it was possible to drill a hole to insert the needle. This has important consequences as
233 dense and well consolidated rocks that can have a higher thermal conductivity tend to be more
234 suitable for measurements than soft and friable rocks that can have a lower thermal
235 conductivity. When showing visible porosity, the samples were immersed in water 48 hours
236 prior to testing for saturation. Thermal conductivity was assumed isotropic for each
237 measurement. Alternatively, dry measurements were performed. A thermal grease compound
238 was applied on the needle to ensure good contact between the needle and the samples.

239 Thermal conductivity measurements were conducted in the laboratory at room temperature
240 according to the ASTM D5334 methodology (ASTM International 2008). The probe was
241 initially inserted in a reference polyethylene standard of known thermal conductivity equal to
242 $0.37 \text{ W m}^{-1} \text{ K}^{-1}$ and heat was injected once during a period of approximately five minutes
243 followed by five minutes of thermal recovery to make a measurement. The probe was then
244 inserted in a rock sample and heat injection was repeated every hour to make at least five
245 consecutive thermal conductivity measurements and allow sufficient cooling time between
246 each measurement. A reference sample measurement was repeated after the series of rock
247 sample measurements. The two reference sample measurements were averaged to determine a
248 correction factor that is multiplied to the rock sample measurements that are finally averaged
249 to return the final thermal conductivity of the rock sample. This procedure was repeated for
250 each forty-five samples tested.

251 The thermal conductivity was determined from the heat injection experiments with the slope
252 method originating from a simplification of the infinite line source equation:

$$253 \quad \lambda = \frac{q}{4\pi m} \quad \text{eq. 1}$$

254 where λ ($\text{W m}^{-1} \text{ K}^{-1}$) is the thermal conductivity, q (W m^{-1}) is the heat injection rate and m is
255 the slope determined from the late temperature increments plotted as function of the

256 logarithmic time. In the analysis of recovery data, the temperature increments are plotted as
 257 function of a normalized logarithmic time (t/t_c) to determine the slope, where t_c (s) is the time
 258 after heat injection stopped. This time normalization originates from the application of the
 259 superposition principle to the infinite line-source equation to reproduce recovery
 260 measurements. The two thermal conductivity estimates obtained from the heat injection and
 261 recovery data were averaged to provide a single measurement per analysis cycle. The
 262 accuracy of the measurements provided by the manufacturer of the needle probe is $\pm 10\%$.

263 Identification of the volumetric heat capacity for each sample was necessary to find the
 264 thermal diffusivity, defined by the ratio of the thermal conductivity over the volumetric heat
 265 capacity, and continue to the next step, in which sizing calculations are performed for a
 266 typical geothermal system. Thin sections of each rock sample were consequently prepared and
 267 analyzed under a petrographic microscope to estimate the main mineralogical phases and the
 268 porosity. This data was used to calculate the volumetric heat capacity of the rock samples
 269 (Waples and Waples 2004b):

$$270 \quad \rho_{rock}Cp_{rock} = \rho_{solids}Cp_{solids}(1 - n) + \rho_{water}Cp_{water}n \quad \text{eq. 2.}$$

271 where ρ (kg m^{-3}) is the density, Cp is the specific heat capacity at constant pressure
 272 ($\text{J kg}^{-1} \text{K}^{-1}$) and n (-) is the porosity fraction. The volumetric heat capacity of the main mineral
 273 phases were averaged according to their volume fraction to find the volumetric heat capacity
 274 of the solids (Waples and Waples 2004a). This approach used to calculate the volumetric heat
 275 capacity yields an approximation whose error has little impact since heat capacity is fairly
 276 similar among rock types and the sensitivity of heat storage to the sizing equation is low.

277 3.3 Geothermal potential evaluation

278 GHEs are an expensive component of ground-coupled heat pump systems. Host rocks in
 279 which fewer GHEs can be installed to offer the same heat transfer potential can be identified
 280 as favorable. Sizing calculations were consequently performed to determine the length of
 281 GHE that would be needed for a small size building, keeping the same design parameters and
 282 changing the subsurface thermal properties according to those found for each sample.

283 The method given by Philippe et al. (2010) for a system with a single borehole was used to
 284 determine the length L (m) of the GHE with:

$$285 \quad L = \frac{q_h R_b + q_y R_{10y} + q_m R_{1m} + q_h R_{6h}}{T_m - T_g} \quad \text{eq. 3}$$

286 where q_h , q_m and q_y (W) are the heat exchange rates with the subsurface, or the ground loads,
287 determined for the maximum hourly load, the monthly average of the design month and the
288 average yearly value, respectively. The effective ground thermal resistances R_{10y} , R_{1m} and
289 R_{6h} ($m K W^{-1}$) are calculated for a ten year, a ten year plus one month and a ten year plus one
290 month and six hours pulses based on the cylindrical-source equation affected by the
291 subsurface thermal properties (Carslaw 1945; Ingersoll et al. 1954). The term R_b ($m K W^{-1}$)
292 denotes the borehole thermal resistance associated to the ground heat exchanger and was
293 evaluated with Hellström's line-source method (1991) using a two-dimensional approach. The
294 temperatures at the dominator T_m and T_g (K) are averages for the water in the GHE and the
295 undisturbed subsurface.

296 The design parameters that were kept constant for each calculation are those of a small
297 residential building with a single GHE that could be a house located in the SLL (Table 1). The
298 system is sized according to heating loads, which are negative for heat to be extracted from
299 the subsurface. The peak heating load imposed to the ground is 7.5 kW, representing a peak
300 heating capacity of 10.5 kW (3 tons) for the building when considering a coefficient of
301 performance equal to 3.5 for the heat pump. The GHE fluid is for water mixed with 25 %
302 propylene glycol providing a $-10\text{ }^\circ\text{C}$ freeze protection and a minimum heat pump inlet
303 temperature of $-2\text{ }^\circ\text{C}$ have been selected. The borehole characteristics are those of typical
304 GHE installed in the SLL made with a single U-pipe having space clips and inserted in
305 0.152 m diameter borehole that is filled with thermally enhanced grout made of quartz sand
306 and bentonite. The subsurface temperature was assumed to be $8\text{ }^\circ\text{C}$ and inferred from maps of
307 Majorowicz et al. (2009). This temperature is a rough average for the study area that is
308 assumed constant at each location since the calculations are performed to identify the effect of
309 the subsurface thermal properties on the required borehole length.

310 The sizing calculations were repeated according to the thermal conductivity and heat capacity
311 determined for each sample in the laboratory. The borehole lengths obtained were classified
312 in three categories, short, medium and long, assigned to a high, medium and low geothermal
313 potential, respectively. The geothermal potential was associated to each sample rather than to
314 thermostratigraphic units since there can be different potential within heterogeneous rocks
315 grouped in a unit. This approach is suitable to identify prominent trends within units and
316 compare rock types of a given area among each other, bearing in mind that the potential is
317 relative to the range of thermal conductivity obtained for the study area.

Table 1. Constant design parameters considered for sizing calculations

Parameter	Unit	Value
Peak hourly ground load	W	-7500
Monthly ground load	W	-3750
Yearly average ground load	W	-998
Undisturbed subsurface temperature	°C	8
Fluid heat capacity	J kg ⁻¹ K ⁻¹	3930
Total mass flow rate per W of peak hourly ground load	kg s ⁻¹ W ⁻¹	78
Minimum heat pump inlet temperature	°C	-2
Borehole radius	M	0.076
Pipe inner radius	M	0.0172
Pipe outer radius	M	0.0210
Grout thermal conductivity	W m ⁻¹ K ⁻¹	1.73
Pipe thermal conductivity	W m ⁻¹ K ⁻¹	0.40
Center to center distance between pipes	M	0.10
Internal convection coefficient	W m ⁻² K ⁻¹	3200

318 **3.4 Map preparation**

319 Although forty-five samples were collected and analyzed in the laboratory to classify the
320 thermostratigraphic units of the SLL basin, those were insufficient to interpolate thermal
321 conductivity assessments between samples. The area covered by the SLL basin in Quebec is
322 roughly 20 000 km² and a very important number of samples would have to be collected to
323 interpolate thermal conductivity measurements with geostatistical methods. The sample
324 locations were consequently plotted, with a dot size proportional to the thermal conductivity
325 measured in the laboratory, on a geological map showing the formations of the sedimentary
326 sequence in background to illustrate the ability of the host rock to transfer heat by conduction.
327 A second dot map was prepared showing the thermostratigraphic units and the geothermal
328 potential determined from the borehole lengths with each sample using superimposed color
329 hexagons and circles to illustrate the favorability to ground-coupled heat pump systems. The
330 resulting maps provide a first data set to help geothermal system designers to find information
331 about the host rock thermal conductivity and conductive heat transfer potential for closed-
332 loop geothermal systems in the SLL basin.

333 **4 Results**

334 The range in thermal conductivity measured on the forty-five samples varies from 2.0 to
335 6.9 W m⁻¹ K⁻¹, with a mean and standard deviation respectively equal to 3.57 and
336 1.46 W m⁻¹ K⁻¹ (Table 2). The obtained thermal conductivity values are described for each
337 thermostratigraphic unit with respect to the distribution of laboratory measurements specific

338 to the SLL basin and the range of values commonly expected for sedimentary rocks (Clauser
339 2014b).

340 The Grenvillian basement below the sedimentary sequence has low to high thermal
341 conductivity ranging from 2.3 to 4.2 W m⁻¹ K⁻¹, which can be explained by varying quartz and
342 plagioclase content. Despite the limited number of samples, rocks of the Grenville were
343 classified in a thermostratigraphic unit since its variability contrast to that of the SLL
344 sedimentary rocks.

345 The Potsdam sandstone at the base of the sedimentary sequence shows the highest thermal
346 conductivity, typically above 6.0 W m⁻¹ K⁻¹. The high quartz content of the Cairnside
347 Formation is responsible for the peak thermal conductivity values of the sedimentary
348 sequence. Thin sections analyses of samples collected in this study revealed a quartz content
349 above 85 % for the Cairnside and Covey Hill formations, explaining the high thermal
350 conductivity. Both formations, the Cairnside and the Covey Hill, have therefore been
351 classified in a single thermostratigraphic unit.

352 The overlying Theresa Formation dominantly made of sandstones similarly has a high thermal
353 conductivity, with two samples having values of 4.0 and 5.9 W m⁻¹ K⁻¹. The transition toward
354 dolostone in the Beauharnois Formation has a strong effect on thermal conductivity
355 decreasing toward moderate values ranging from 2.7 to 4.2 W m⁻¹ K⁻¹. The Theresa and the
356 Beauharnois formations, although in the same geological group, have been classified in two
357 distinct thermostratigraphic units because of the increase in dolomite concentration toward the
358 top. The thermal conductivity of the Theresa Formation is generally intermediate between the
359 Potsdam Group and the Beauharnois Formation, showing a transition that justifies the
360 classification in distinct thermostratigraphic units.

Table 2. Thermal properties and geothermal potential of thermostratigraphic units

Thermostratigraphic unit	Sample number	Lithology	Thermal conductivity (W m ⁻¹ K ⁻¹)	Thermal diffusivity (m ² j ⁻¹)	Borehole length (m)	Geothermal potential
Appalachians	14MN38	Siltstone	3.41	0.14	141	M
	14MN40	Siltstone	3.74	0.23	139	M
	14MN41	Limestone	2.60	0.10	163	L
Queenston and Lorraine	14MN24	Siltstone	2.96	0.11	151	M
	09EK330	Siltstone	3.40	0.13	140	M
	14MN21	Mudstone	2.70	0.10	159	M
	14MN23	Mudstone	2.93	0.11	152	M
	09EK326	Mudstone	2.00	0.08	189	L
	09EK333	Siltstone	3.33	0.13	142	M
	09EK344	Siltstone	3.00	0.12	150	M
Sainte-Rosalie and Utica	14MN35	Mudstone	2.26	0.08	176	L
	14MN36	Siltstone	4.10	0.17	128	H
	09EK335	Arg. dolostone	2.29	0.08	173	L
	14MN27	Siltstone	2.52	0.09	165	L
	14MN29	Siltstone	2.30	0.09	174	L
	14MN30	Mudstone	2.00	0.07	189	L
Trenton, Black River and Chazy	14MN10	Limestone	2.71	0.10	159	M
	14MN13*	Arg. limestone	2.98	0.11	150	M
	14MN14	Limestone	2.63	0.10	161	L
	14MN17	Limestone	2.50	0.09	166	L
	14MN19*	Limestone	3.20	0.12	144	M
	14MN28	Arg. limestone	2.63	0.10	162	L
	14MN31	Arg. limestone	2.60	0.10	163	L
	14MN32	Arg. limestone	2.67	0.10	161	L
	09EK311	Arg. limestone	2.60	0.10	162	L
	09EK320	Limestone	2.60	0.10	162	L
	09EK324	Limestone	4.15	0.17	127	H
Beekmantown (Beauharnois)	14MN09	Limestone	2.70	0.10	159	M
	14MN11	Dolostone	2.85	0.11	154	M
	14MN12	Dolostone	4.24	0.15	124	H
	14MN20	Dolostone	3.48	0.12	137	M
	09EK304	Dolostone	3.60	0.13	135	M
Beekmantown (Theresa)	14MN01*	Sandstone	5.88	0.22	107	H
	14MN16	Sandstone	4.00	0.16	129	H
Potsdam	14MN02*	Sandstone	6.90	0.29	101	H
	14MN03*	Sandstone	6.67	0.27	102	H
	14MN04*	Sandstone	6.43	0.24	103	H
	14MN05*	Sandstone	6.43	0.23	110	H
	14MN06*	Sandstone	6.31	0.27	105	H
	14MN07*	Sandstone	6.55	0.28	103	H
	14MN08*	Sandstone	6.05	0.24	106	H
Grenville	14MN18	Igneous	2.25	0.09	178	L
	14MN33	Igneous	2.71	0.11	160	L
	14MN34	Igneous	2.51	0.12	170	L
	09EK341	Igneous	4.18	0.17	127	H

Abbreviations for the geothermal potential: L; low ≥ 160 m, M; moderate > 130 m < 160 m, H; high ≤ 130 m.

Arg.: argillaceous. * Sample with visible porosity that has been saturated for thermal conductivity measurement.

361 The change in mineralogy originating from the depositional environment resulting in
362 dominant limestone content with some clay for the Trenton, Black River and Chazy groups
363 have a strong effect on thermal conductivity ranging from 2.5 to 4.2 W m⁻¹ K⁻¹. Observations
364 indicate that thermal conductivity of limestone and argillaceous limestone is most commonly
365 between 2.5 to 3.0 W m⁻¹ K⁻¹, and can occasionally be higher in sedimentary beds containing
366 dolomite and quartz. Dolomite and sandstone layers, mostly found at the base in the Chazy
367 Group, are thinner than those of the limestone and argillaceous limestone layers and the three
368 groups, Trenton, Black River and Chazy, have therefore been classified in a single
369 thermostratigraphic unit.

370 The increase in clay content in the Utica Shale and the Sainte-Rosalie Group affects the
371 thermal conductivity that is generally below 2.5 W m⁻¹ K⁻¹ in those two geological units. A
372 low value of 2.0 W m⁻¹ K⁻¹ has been observed in the Utica Shale. One sample with a high
373 thermal conductivity of 4.1 W m⁻¹ K⁻¹ was found in the Sainte-Rosalie Group and was
374 associated with a greater quartz content that is uncommon. The Utica Shale and the Sainte-
375 Rosalie Group were classified in a single thermostratigraphic unit because of their similar low
376 thermal conductivity.

377 Lithologies are variable in the overlying Lorraine and Queenston groups of shallow marine to
378 continental depositional environment, which affects thermal conductivity values that are
379 generally moderate and range from 2.0 to 3.4 W m⁻¹ K⁻¹. Shale is the dominant lithology and
380 is mixed with other rock types, explaining the variations in thermal conductivity for those two
381 groups that have been classified in a single thermostratigraphic unit. Samples collected for the
382 proximal Appalachians have a thermal conductivity that is similar to that of the adjacent
383 Lorraine Group. Major faults separate the Appalachians from the Lorraine Group and the
384 Appalachians have been classified in a distinct thermostratigraphic unit.

385 The borehole length calculated for a typical geothermal system of small size with the thermal
386 properties measured in the laboratory reveals the geothermal potential of each sample and the
387 dominant trend for the thermostratigraphic units (Table 2). A high, moderate and low
388 geothermal potential for closed-loop systems has been assigned to borehole lengths less than
389 or equal to 130 m, between 130 to 160 m and greater or equal to 160 m, respectively. The
390 samples with a low, medium and high geothermal potential show a thermal conductivity less
391 than 2.7 W m⁻¹ K⁻¹, between 2.7 and 3.7 W m⁻¹ K⁻¹, and above 4.0 W m⁻¹ K⁻¹, respectively.
392 The thermostratigraphic units with samples having a dominantly high thermal conductivity,
393 such as the Potsdam Group and the Theresa Formation, have a most frequently high

394 geothermal potential. The thermostratigraphic units with samples of mainly low thermal
395 conductivity, like the Utica Shale and the Sainte-Rosalie Group, have a most frequently low
396 geothermal potential, although punctual deviation characteristic of heterogeneity was
397 observed.

398 The thermal conductivity measurements and the associated thermostratigraphic units plotted on
399 the geological map (Figures 3a and b) suggest a high geothermal potential in the Southwest of
400 the SLL basin, where rocks of the Potsdam Group and the Theresa Formation are found near
401 the surface. Toward the Northeast of the SLL basin, the basal sandstones are buried below the
402 Trenton, Black River, Chazy, Utica and Sainte-Rosalie groups with a lower geothermal
403 potential. A moderate geothermal potential associated to the Lorraine and Queenston groups
404 is more common at the center of the synclinal defining the dominant geological structure in
405 the SLL basin.

406 It is important to recall that thermal conductivity measurements made with a needle probe can
407 be difficult to realize for friable rocks composed of shale of low thermal conductivity.
408 Consequently, laboratory measurements may be slightly higher than in situ measurements.
409 Additionally, the comparison made between the thermostratigraphic units is relative to the
410 range of values obtained for the study area. Thermal conductivity measurements below
411 $2.5 \text{ W m}^{-1} \text{ K}^{-1}$ were classified in this work as low, especially when compared to quartz rich
412 sandstone of thermal conductivity greater than $6.0 \text{ W m}^{-1} \text{ K}^{-1}$, but could be considered as
413 moderate when taking into account the range of thermal conductivity observed for geological
414 materials that can be as low as $0.6 \text{ W m}^{-1} \text{ K}^{-1}$.

415 **5 Discussion**

416 Thermostratigraphy, which can be considered as a stratigraphic concept such as
417 lithostratigraphy or biostratigraphy, focuses on the links between rock sequences, including
418 their origin and composition, and thermal property variations, mainly thermal conductivity. It
419 can be used to tie subsurface temperature profiles to thermal conductivity and heat flux with
420 the application of Fourier's law for heat conduction. The use of thermostratigraphic principles
421 is common in the study of terrestrial heat flow and the assessment of deep geothermal
422 resources for power generation. For example, Gosnold et al. (2012) extrapolated temperature
423 at depth in the Williston basin of North Dakota with thermostratigraphic principles making
424 use of heat flow assessments and thermal conductivity measurements. Other recent examples
425 of thermostratigraphic assessment in the context of deep geothermal resources evaluation in

426 sedimentary basins of the United States have been described by Gosnold et al. (2010),
427 Crowell and Gosnold (2011) and Crowell et al. (2011).

428 Rock thermosequences were further involved in the definition of thermofacies presented by
429 Sass and Götz (2012) for the exploration of geothermal reservoirs to produce electricity. The
430 concept is to compare thermal conductivity and permeability of rock samples to classify rock
431 units of a geothermal system from petrothermal, or conductive heat transfer dominated, to
432 hydrothermal, or convective heat transfer dominated. This principle has been applied in
433 various geological environments, for example the Molasse sedimentary Basin in Germany
434 (Homuth et al. 2015), the Tauhara hydrothermal field in New Zealand (Mielke et al. 2015)
435 and volcanoclastics of the Valley of Mexico (Lenhardt and Götz 2015). Aretz et al. (2016)
436 presented a recent study where depositional environments and diagenesis processes are linked
437 to thermal and hydraulic properties in geothermal reservoirs of sedimentary origin.

438 A similar attempt to classify rock thermosequences, but in the scope of shallow geothermal
439 resources for ground-coupled heat pump systems, is presented in this study. The
440 thermostratigraphic units, defined as consecutive geological layers of similar conductive heat
441 transfer potential, links the geological environment to mineralogy changes and the resulting
442 subsurface thermal conductivity. It can be used to define favorability to geothermal heat
443 pumps at a regional scale, where interpolation between thermal conductivity measurements is
444 difficult for large territories. The results presented on point maps are an alternative to
445 assigning thermal conductivity ranges to geological units, for example done by Di Sipio et al.
446 (2014), when thermal conductivity variations are important, likely more than $0.5 \text{ W m}^{-1} \text{ K}^{-1}$
447 within a unit. The thermostratigraphic assessment presented in this study can help to design
448 ground-coupled heat pumps that dominantly operate under conductive heat transfer with the
449 subsurface. Thermal conductivity values can be used as a basis for geothermal potential
450 assessment according to geothermal heat pump simulations (Galgaro et al., 2015), in which
451 valuable results are supported by field data. Simple sizing calculations with inputs from
452 laboratory measurements of thermal conductivity were used in this study to evaluate the
453 length of GHE needed for a given heat pump system to define the geothermal potential. The
454 assessment provided classes and thermal conductivity ranges for thermostratigraphic units to
455 be used in the absence of a thermal response test to design systems. The concept is not to
456 replace in situ measurements of the subsurface thermal conductivity but to use this assessment
457 to guide design of small systems, where a field test can be uneconomic (Robert and Gosselin
458 2014), or for screening calculations of larger systems, where a test can be performed

459 afterward to validate field conditions. A designer could use the map provided in this study to
460 locate its geothermal system and infer the possible thermal conductivity for the bedrock
461 encountered. The thickness of the overburden and its thermal conductivity, which can be
462 estimated from databases of the geological records, shall be considered for a complete
463 assessment of the subsurface over the depth of the planned borehole. Nevertheless, the maps
464 presented provide information about the thermal conductivity of the bedrock, an essential
465 parameter to design and simulate geothermal systems that was until now difficult to evaluate
466 in the SLL basin.

467 **6 Conclusions**

468 The geothermal heat pump potential of the St. Lawrence Lowlands (SLL) basin was evaluated
469 based on a first thermostratigraphic assessment of rock sequences located in Quebec, Canada.
470 Sizing calculations performed to determine the length of a ground heat exchanger for a small
471 residential building, according to thermal properties measured in the laboratory on rock
472 samples collected in outcrops, provided the basis to determine the favorability of geothermal
473 heating and cooling systems. The analysis revealed a high geothermal potential for basal
474 sandstones of the Potsdam Group that formed in a rift environment. The high quartz content is
475 responsible for the high thermal conductivity of those sandstones. The overlying rock units of
476 the Theresa and Beauharnois formations, the Chazy, Black River and Trenton groups as well
477 as the Utica Shale and the Sainte-Rosalie Group deposited in a passive margin evolving to a
478 foreland basin. The resulting transition of dolostone to argillaceous limestone and then shale
479 exhibited a high to low geothermal potential decreasing toward the top. The change in
480 mineralogy related to the depositional environment is the dominant factor affecting the
481 subsurface thermal conductivity. Turbidites and molasses of the overlying Lorraine and
482 Queenston groups tend to be more heterogeneous and generally had a moderate geothermal
483 potential, although the potential can change laterally and stratigraphically in the sedimentary
484 basin.

485 The present study provides an original contribution to help design geothermal heat pump
486 systems that will be installed in the SLL, where most population is found in the province of
487 Québec. The results showed how to link subsurface thermal properties to mineralogy, rock
488 type and depositional environments to improve geothermal heating and cooling, a human
489 activity that can benefit to the environment with significant energy savings. This geoscientific
490 mapping exercise offers new data downloadable as supplementary material accompanying the
491 paper to help develop green buildings using sustainable energy sources. The regional

492 geothermal potential evaluation was conducted over an area of about 20 000 km² and will be
493 detailed in smaller areas, where the energy needs and the building density are most important.
494 Units of the Grenville and the Appalachians geological provinces, representing regions with
495 significant population when adjacent to the SLL, were studied for comparison with rocks of
496 the SLL basin but will require more samples to picture the diversity of rock types in these
497 complex geological environments. A study focusing on the Grenville and the Appalachians
498 would obviously result in the identification of several thermal conductivity classes. The
499 Beekmantown Group within the SLL basin needs to be studied in more detail to better
500 characterize the transition from high to medium geothermal potential in the Theresa to
501 Beauharnois formations changing from sandstone to dolostone. Lateral facies changes in the
502 basin can be included in further studies to refine the geothermal potential assessment. Next
503 studies will focus on data collection with a higher spatial resolution in smaller areas of greater
504 interest to interpolate thermal properties with geostatistical methods.

505 **7 Acknowledgements**

506 The Bating Postdoctoral Fellowship program, the Natural Sciences and Engineering Research
507 Council of Canada and the *Fonds de recherche du Québec – Nature et technologies* are
508 acknowledged for funding this research.

509 **8 References**

- 510 Al-Khoury R, Bonnier PG (2006) Efficient finite element formulation for geothermal heating
511 systems. Part II: Transient. *Int J Numer Methods Eng* 67:725–745. doi:
512 10.1002/nme.1662
- 513 Al-Khoury R, Bonnier PG, Brinkgreve RBJ (2005) Efficient finite element formulation for
514 geothermal heating systems. Part I: Steady state. *Int J Numer Methods Eng* 63:988–
515 1013. doi: 10.1002/nme.1313
- 516 Aretz A, Bär K, Götz AE, Sass I (2016) Outcrop analogue study of Permocarbiniferous
517 geothermal sandstone reservoir formations (northern Upper Rhine Graben, Germany):
518 impact of mineral content, depositional environment and diagenesis on petrophysical
519 properties. *Int J Earth Sci* 105:1431–1452. doi:10.1007/s00531-015-1263-2
- 520 ASTM International (2008) Standard test method for determination of thermal conductivity of
521 soil and soft rock by thermal needle probe procedure. ASTM International, Harbor
522 Drive
- 523 Bernier M (2001) Ground-coupled heat pump system simulation. *ASHRAE Trans* 107:605–
524 616.
- 525 Bernier M (2000) A Review of the cylindrical heat source method for the design and analysis
526 of vertical ground-coupled heat pump systems. In: *Proceedings of the Fourth*

- 527 International Conference on Heat Pumps in Cold Climates Conference, Caneta
528 Research Inc., Aylmer, pp 1–14
- 529 Brisebois D, Brun J (1994) La plate-forme du Saint-Laurent et les Appalaches. In: Géologie
530 du Québec, Ministère des ressources naturelles (ed.), Gouvernement du Québec,
531 Quebec City.
- 532 Canadian GeoExchange Coalition (2012) The state of the Canadian geothermal heat pump
533 industry 2011 - Industry survey and market analysis. Canadian GeoExchange
534 Coalition, Montreal, Available on the Internet : [http://www.geo-](http://www.geo-exchange.ca/en/UserAttachments/article81_Final%20Stats%20Report%202011%20-%20February%206,%202012_E.pdf)
535 [exchange.ca/en/UserAttachments/article81_Final%20Stats%20Report%202011%20-](http://www.geo-exchange.ca/en/UserAttachments/article81_Final%20Stats%20Report%202011%20-%20February%206,%202012_E.pdf)
536 [%20February%206,%202012_E.pdf](http://www.geo-exchange.ca/en/UserAttachments/article81_Final%20Stats%20Report%202011%20-%20February%206,%202012_E.pdf)
- 537 Casasso A, Sethi R (2016) G.POT: A quantitative method for the assessment and mapping of
538 the shallow geothermal potential. *Energy* 106, 765–773.
539 doi:10.1016/j.energy.2016.03.091
- 540 Carrier M-A, Lefebvre R, Rivard C, et al (2013) Portrait des ressources en eau souterraine
541 en Montérégie Est, Québec, Canada. Institut national de la recherche scientifique -
542 Centre Eau Terre Environnement, Quebec City, Available on the Internet :
543 <http://espace.inrs.ca/1639/1/R001433.pdf>
- 544 Carslaw HS (1945) Introduction to the mathematical theory of the conduction of heat in
545 solids. Dover, New York
- 546 Castonguay S, Lavoie D, Dietrich J, Laliberté J-Y (2010) Structure and petroleum plays of the
547 St. Lawrence Platform and Appalachians in southern Quebec: insights from
548 interpretation of MRNQ seismic reflection data. *Bull Can Pet Geol* 58:219–234.
549 doi:10.2113/gscpgbull.58.3.219
- 550 Clauser C (2006) Geothermal energy. In: Heinloth K (ed) Landolt-Börnstein, Group VII:
551 Advanced Materials and Technologies, Vol. 3: Energy Technologies, Subvol. C:
552 Renewable Energies. Springer, Heidelberg-Berlin, pp 493–604
- 553 Clauser C (2014a) Thermal Storage and Transport Properties of Rocks, I: Heat Capacity and
554 Latent Heat. In: Gupta H (ed) Encyclopedia of Solid Earth Geophysics. Springer
555 Netherlands, pp 1423–1431
- 556 Clauser C (2014b) Thermal Storage and Transport Properties of Rocks, II: Thermal
557 Conductivity and Diffusivity. In: Gupta H (ed) Encyclopedia of Solid Earth
558 Geophysics. Springer, Netherlands, pp 1431–1448
- 559 Clauser C, Huenges E (1995) Thermal conductivity of rocks and minerals. In: Ahrens TJ (ed)
560 Rock physics & phase relations; a handbook of physical constants, AGU Reference
561 Shelf. American Geophysical Union, Washington DC, pp 105–126
- 562 Comeau F-A, Bédard K, Malo M (2012) Lithostratigraphie standardisée du bassin des Basses-
563 Terres du Saint-Laurent basée sur l'étude des diagraphies. Institut national de la
564 recherche scientifique - Centre Eau Terre Environnement, Quebec City, Available on
565 the Internet : <http://espace.inrs.ca/1645/1/R001442.pdf>

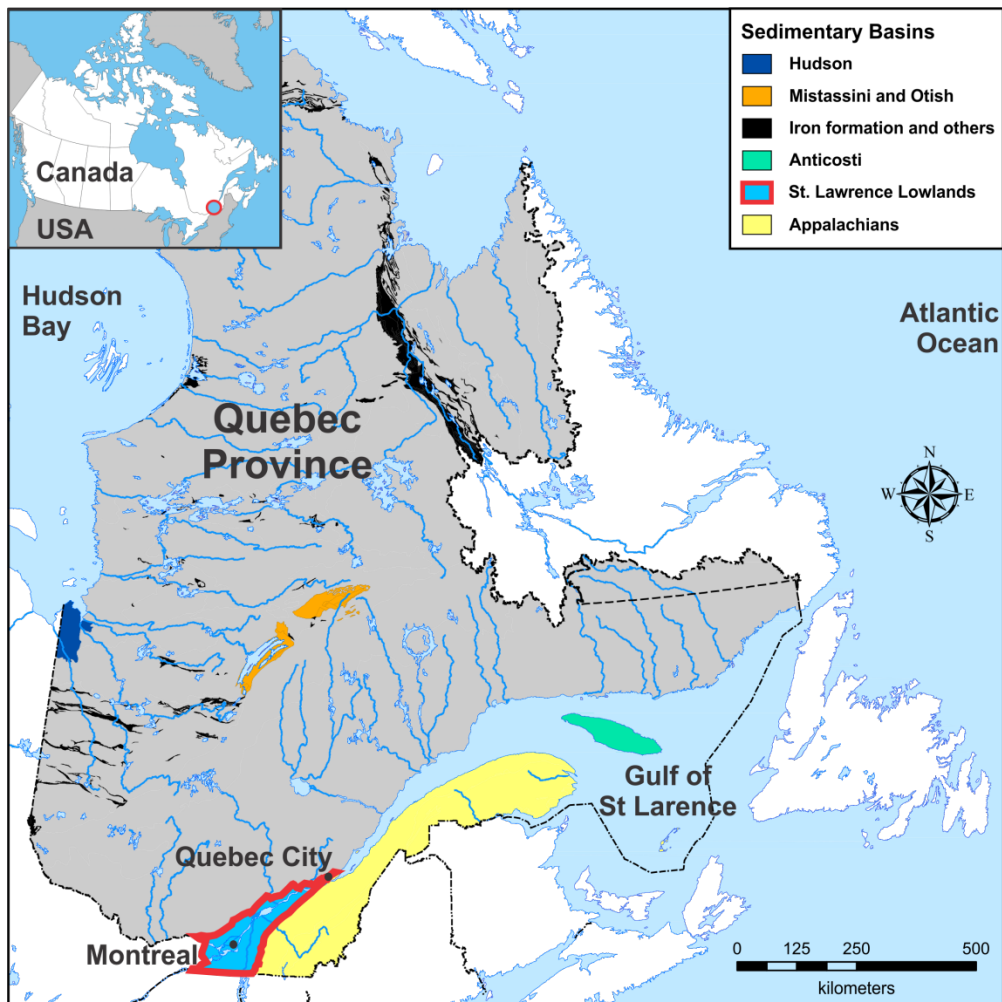
- 566 Crowell A, Gosnold W (2011) Correcting bottom-hole temperatures: a Look at the Permian
567 Basin (Texas), Anadarko and Arkoma Basins (Oklahoma), and Williston Basin (North
568 Dakota). *GRC Trans* 35:735–738.
- 569 Crowell A, Klenner R, Gosnold W (2011) GIS analysis for the volumes, and available energy
570 of selected reservoirs: Williston Basin, North Dakota. *GRC Trans* 35:1557–1562.
- 571 Cui P, Yang H, Spitler JD, Fang Z (2008) Simulation of hybrid ground-coupled heat pump
572 with domestic hot water heating systems using HVACSIM+. *Energy Build* 40:1731–
573 1736. doi: 10.1016/j.enbuild.2008.03.001
- 574 De Filippis G, Margiotta S, Negri S, Giudici M, 2015. The geothermal potential of the
575 underground of the Salento peninsula (southern Italy). *Environ Earth Sci* 73, 6733–
576 6746. doi:10.1007/s12665-014-4011-1
- 577 Di Sipio E, Galgaro A, Destro E, et al (2014) Subsurface thermal conductivity assessment in
578 Calabria (southern Italy): a regional case study. *Environ Earth Sci* 72:1383–1401. doi:
579 10.1007/s12665-014-3277-7
- 580 Galgaro A, Di Sipio E, Teza G, Destro E, De Carli M, Chiesa S, Zarrella A, Emmi G,
581 Manzella A (2015) Empirical modeling of maps of geo-exchange potential for shallow
582 geothermal energy at regional scale. *Geothermics* 57, 173–184.
583 doi:10.1016/j.geothermics.2015.06.017
- 584 Gehlin S, Nordell B (2003) Determining undisturbed ground temperature for thermal response
585 test. *ASHRAE Trans* 109:151–156.
- 586 Globensky Y (1987) Géologie des Basses-Terres du Saint-Laurent. Ministère de l'Énergie et
587 des Ressources du Québec, Quebec City
- 588 Gosnold WD, McDonald MR, Klenner R, Merriam D (2012) Thermostratigraphy of the
589 Williston Basin. *GRC Trans* 36:663–670.
- 590 Gosnold W, LeFever R, Mann M, et al (2010) EGS potential in the northern midcontinent of
591 North America. *GRC Trans* 34:355–358.
- 592 Hellström G (1991) Ground heat storage; thermal analysis of duct storage systems. Ph.D.
593 Thesis, Department of mathematical physics, University of Lund, Lund, Available on
594 the Internet :
595 [http://lup.lub.lu.se/luur/download?func=downloadFile&recordOid=2536279&fileOid=](http://lup.lub.lu.se/luur/download?func=downloadFile&recordOid=2536279&fileOid=8161230)
596 [8161230](http://lup.lub.lu.se/luur/download?func=downloadFile&recordOid=2536279&fileOid=8161230)
- 597 Homuth S, Götz AE, Sass I (2015) Reservoir characterization of the Upper Jurassic
598 geothermal target formations (Molasse Basin, Germany): role of thermofacies as
599 exploration tool. *Geoth Energ Sci* 3:41–49. doi: 10.5194/gtes-3-41-2015
- 600 Ingersoll LR, Zobel OJ, Ingersoll AC (1954) Heat conduction, with engineering, geological,
601 and other applications. McGraw-Hill, New York
- 602 Lamarche L (2009) A fast algorithm for the hourly simulations of ground-source heat pumps
603 using arbitrary response factors. *Renew Energy* 34:2252–2258.
604 doi:10.1016/j.renene.2009.02.010

- 605 Lamarche L, Beauchamp B (2007a) New solutions for the short-time analysis of geothermal
606 vertical boreholes. *Int J Heat Mass Transf* 50:1408–1419. doi:
607 10.1016/j.ijheatmasstransfer.2006.09.007
- 608 Lamarche L, Beauchamp B (2007b) A new contribution to the finite line-source model for
609 geothermal boreholes. *Energy Build* 39:188–198. doi: 10.1016/j.enbuild.2006.06.003
- 610 Laroque M, Gagné S, Barnetche D, et al (2015) Projet de connaissance des eaux souterraines
611 du bassin versant de la zone Nicolet et de la partie basse de la zone Saint-François.
612 Université du Québec à Montréal, Montreal, Available on the Internet : [http://rqes-](http://rqes-gries.ca/upload/files/Rapports/PACES-Phase-3/NSF/Rapport_NSF_Phase_III_Final_tailler%C3%A9duite_Partie1.pdf)
613 [gries.ca/upload/files/Rapports/PACES-Phase-](http://rqes-gries.ca/upload/files/Rapports/PACES-Phase-3/NSF/Rapport_NSF_Phase_III_Final_tailler%C3%A9duite_Partie1.pdf)
614 [3/NSF/Rapport_NSF_Phase_III_Final_tailler%C3%A9duite_Partie1.pdf](http://rqes-gries.ca/upload/files/Rapports/PACES-Phase-3/NSF/Rapport_NSF_Phase_III_Final_tailler%C3%A9duite_Partie1.pdf)
- 615 Lavoie D (1994) Diachronous tectonic collapse of the Ordovician continental margin, eastern
616 Canada: comparison between the Quebec reentrant and St. Lawrence Promontory. *Can*
617 *J Earth Sci* 31:1309-1319. doi: 10.1139/e94-113
- 618 Lee CK, Lam HN (2008) Computer simulation of borehole ground heat exchangers for
619 geothermal heat pump systems. *Renew Energy* 33:1286–1296. doi:
620 10.1016/j.renene.2007.07.006
- 621 Lenhardt N, Götz AE (2015) Geothermal reservoir potential of volcanoclastic settings: The
622 Valley of Mexico, Central Mexico. *Renew Energy* 77:423–429. doi:
623 10.1016/j.renene.2014.12.034
- 624 Li S, Dong K, Wang J, Zhang X (2015) Long term coupled simulation for ground source heat
625 pump and underground heat exchangers. *Energy Build* 106:13–22. doi:
626 10.1016/j.enbuild.2015.05.041
- 627 Li Z, Zheng M (2009) Development of a numerical model for the simulation of vertical U-
628 tube ground heat exchangers. *Appl Therm Eng* 29:920–924.
629 doi:10.1016/j.applthermaleng.2008.04.024
- 630 Majorowicz JA, Grasby SE, Skinner WC (2009) Estimation of shallow geothermal energy
631 resource in Canada: heat gain and heat sink. *Nat Resour Res* 18:95–108. doi:
632 10.1007/s11053-009-9090-4
- 633 Mielke P, Nehler M, Bignall G, Sass I (2015) Thermo-physical rock properties and the impact
634 of advancing hydrothermal alteration — A case study from the Tauhara geothermal
635 field, New Zealand. *J Volcanol Geotherm Res* 301:14–28. doi:
636 10.1016/j.jvolgeores.2015.04.007
- 637 Nasr M, Raymond J, Malo M (2015) Évaluation en laboratoire des caractéristiques
638 thermiques du bassin sédimentaire des Basses-Terres du Saint-Laurent. In:
639 *Proceedings of the 68th Canadian Geotechnical Conference and 7th Canadian*
640 *Permafrost Conference, Québec City, 8 pp*
- 641 Ondreka J, Rüsgen MI, Stober I, Czurda K (2007). GIS-supported mapping of shallow
642 geothermal potential of representative areas in south-western Germany—Possibilities
643 and limitations. *Renew Energy* 32, 2186–2200. doi:10.1016/j.renene.2006.11.009

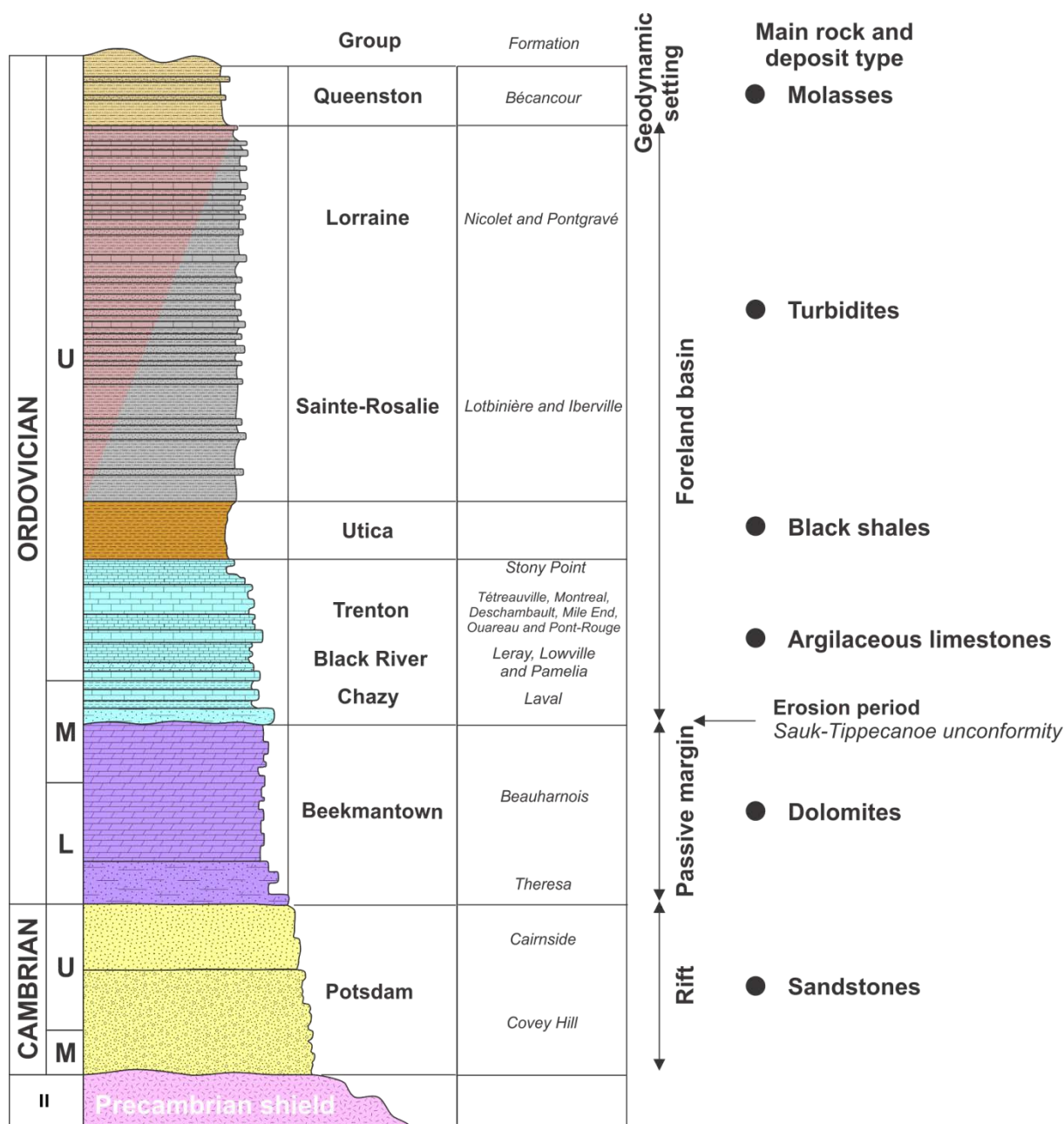
- 644 Philippe M, Bernier M, Marchio D (2009) Validity ranges of three analytical solutions to heat
645 transfer in the vicinity of single boreholes. *Geothermics* 38:407–413.
646 doi:10.1016/j.geothermics.2009.07.002
- 647 Philippe M, Bernier M, Marchio D (2010) Sizing calculation spreadsheet - Vertical
648 geothermal borefields. *ASHRAE J* 52:20–28.
- 649 Rainieri S, Bozzoli F, Pagliarini G (2011) Modeling approaches applied to the thermal
650 response test: A critical review of the literature. *HVACR Res* 17:977–990. doi:
651 10.1080/10789669.2011.610282
- 652 Raymond J, Therrien R, Gosselin L, Lefebvre R (2011) A review of thermal response test
653 analysis using pumping test concepts. *Ground Water* 49:932–945. doi:
654 10.1111/j.1745-6584.2010.00791x
- 655 Robert F, Gosselin L (2014) New methodology to design ground coupled heat pump systems
656 based on total cost minimization. *Appl Therm Eng* 62:481–491. doi:
657 10.1016/j.applthermaleng.2013.08.003
- 658 Santilano A, Manzella A, Donato A, Montanari D, Gola G, Di Sipio E, Destro E, Giaretta A,
659 Galgaro A, Teza G, Viezzoli A, Menghini A, 2015. Shallow Geothermal Exploration
660 by Means of SkyTEM Electrical Resistivity Data: An Application in Sicily (Italy). In:
661 Lollino G, Manconi A, Clague J, Shan W, Chiarle M (Eds.), *Engineering Geology for
662 Society and Territory - Volume 1: Climate Change and Engineering Geology*.
663 Springer International Publishing, Cham, pp. 363–367.
- 664 Sass I, Götz AE (2012) Geothermal reservoir characterization: a thermofacies concept. *Terra
665 Nova* 24:142–147. doi: 10.1111/j.1365-3121.2011.01048.x
- 666 Self SJ, Reddy BV, Rosen MA (2013) Geothermal heat pump systems: Status review and
667 comparison with other heating options. *Appl Energy* 101:341–348.
668 doi:10.1016/j.apenergy.2012.01.048
- 669 Signorelli S, Kohl T (2004) Regional ground surface temperature mapping from
670 meteorological data. *Glob Planet Change* 40:267–284. doi:
671 10.1016/j.gloplacha.2003.08.003
- 672 Spitler JD, Gehlin SEA (2015) Thermal response testing for ground source heat pump
673 systems—An historical review. *Renew Sustain Energy Rev* 50:1125–1137. doi:
674 10.1016/j.rser.2015.05.061
- 675 Tran Ngoc TD, Lefebvre R, Konstantinovskaya E, Malo M (2014) Characterization of deep
676 saline aquifers in the Bécancour area, St. Lawrence Lowlands, Québec, Canada:
677 Implications for CO₂ geological storage. *Environ Earth Sci* 72:119–146. doi:
678 10.1007/s12665-013-2941-7
- 679 Teza G, Galgaro A, Destro E, Di Sipio E (2015). Stratigraphy modeling and thermal
680 conductivity computation in areas characterized by Quaternary sediments.
681 *Geothermics* 57, 145–156. doi:10.1016/j.geothermics.2015.06.016

- 682 Wang S, Liu X, Gates S (2015) An introduction of new features for conventional and hybrid
683 GSHP simulations in eQUEST 3.7. *Energy Build* 105:368–376. doi:
684 10.1016/j.enbuild.2015.07.041
- 685 Waples DW, Waples JS (2004a) A review and evaluation of specific heat capacities of rocks,
686 minerals, and subsurface fluids. Part 1: minerals and nonporous rocks. *Nat Resour Res*
687 13:97–122. doi: 10.1023/B:NARR.0000032647.41046.e7
- 688 Waples DW, Waples JS (2004b) A review and evaluation of specific heat capacities of rocks,
689 minerals, and subsurface fluids. Part 2: fluids and porous rocks. *Nat Resour Res*
690 13:123–130. doi: 10.1023/B:NARR.0000032648.15016.49
- 691 Yang H, Cui P, Fang Z (2010) Vertical-borehole ground-coupled heat pumps: A review of
692 models and systems. *Appl Energy* 87:16–27. doi:10.1016/j.apenergy.2009.04.038

693 Figure and captions

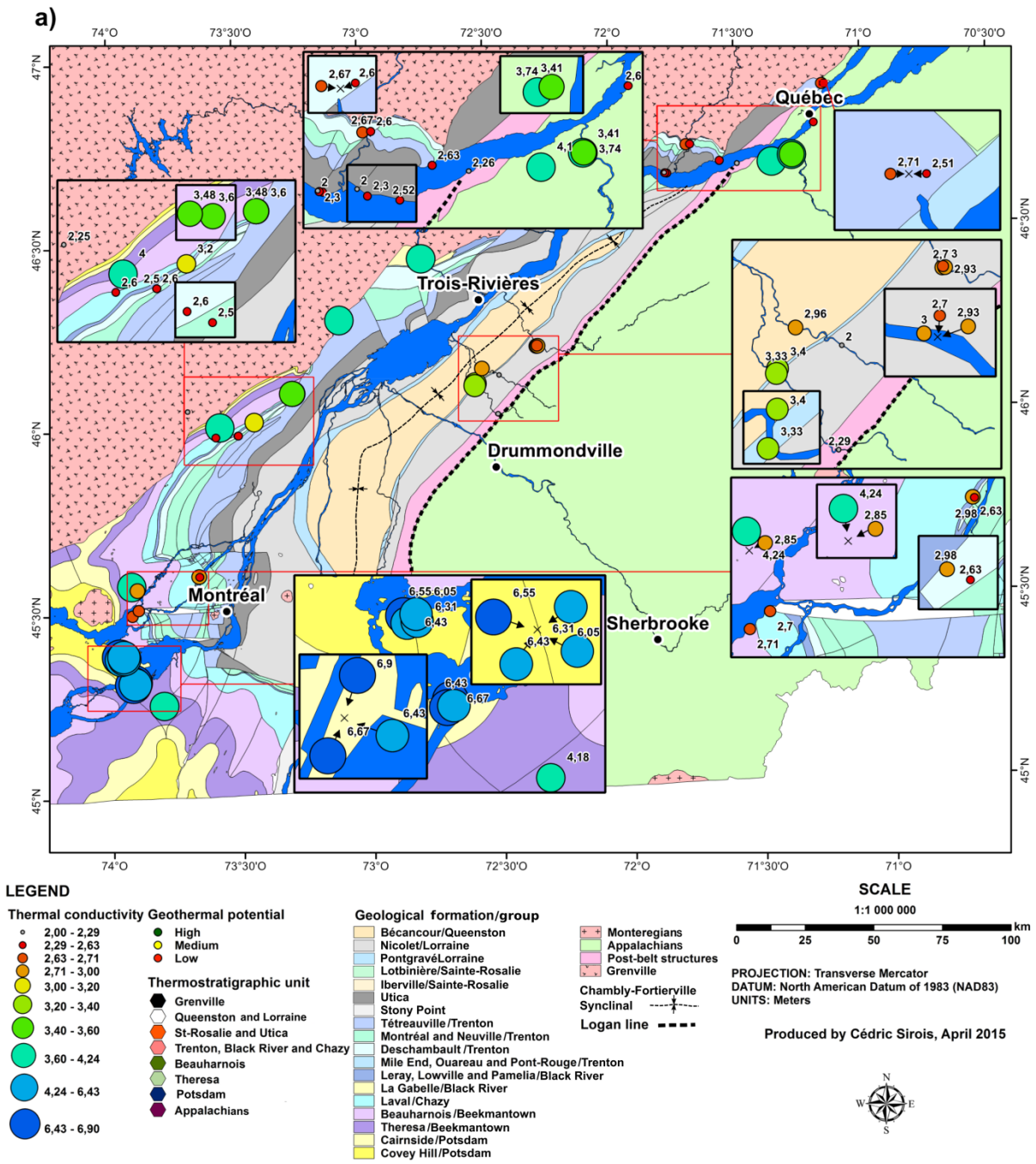


694
695 **Figure 1.** Location of the study area in St. Lawrence Lowlands and other sedimentary basins
696 in the province of Quebec, Canada.

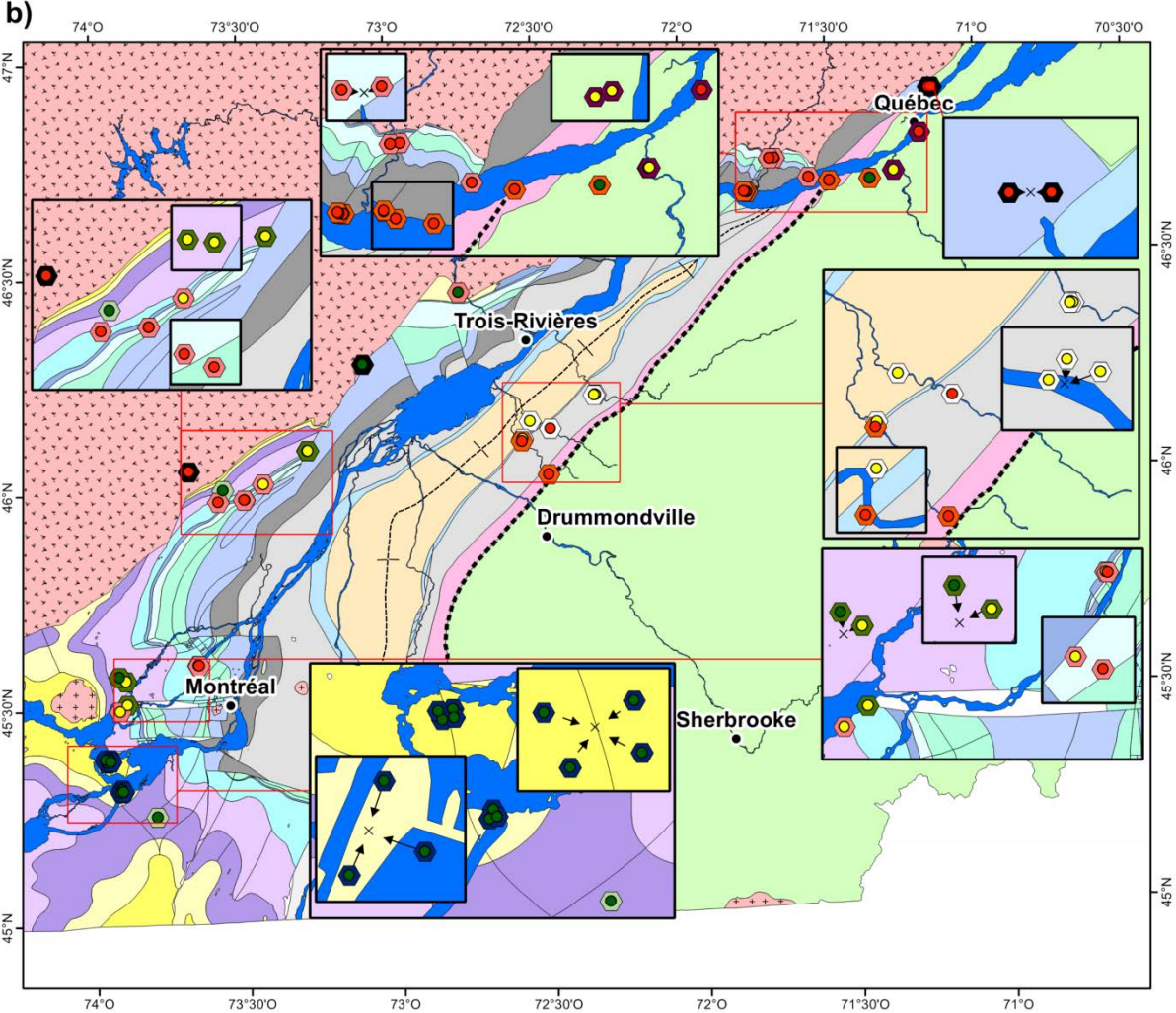


697

698 **Figure 2.** Stratigraphic column showing the St. Lawrence Lowlands sedimentary sequence
699 (Comeau et al. 2012).



700



701

702 **Figure 3.** Geological map of the St. Lawrence Lowlands showing a) thermal conductivity
703 measurements and b) geothermal potential assessment of thermostratigraphic units.